nature cell biology

LETTERS

https://doi.org/10.1038/s41556-018-0068-5

EFF-1 fusogen promotes phagosome sealing during cell process clearance in *Caenorhabditis elegans*

Piya Ghose[1], Alina Rashid[1,3], Peter Insley[1,3], Meera Trivedi[1], Pavak Shah[2], Anupriya Singhal[1], Yun Lu[1], Zhirong Bao[2] and Shai Shaham[1*]

Phagocytosis of dying cells is critical in development and immunity[1–3]. Although proteins for recognition and engulfment of cellular debris following cell death are known[4,5], proteins that directly mediate phagosome sealing are uncharacterized. Furthermore, whether all phagocytic targets are cleared using the same machinery is unclear. Degeneration of morphologically complex cells, such as neurons, glia and melanocytes, produces phagocytic targets of various shapes and sizes located in different microenvironments[6,7]. Thus, such cells offer unique settings to explore engulfment programme mechanisms and specificity. Here, we report that dismantling and clearance of a morphologically complex *Caenorhabditis elegans* epithelial cell requires separate cell soma, proximal and distal process programmes. Similar compartment-specific events govern the elimination of a *C. elegans* neuron. Although canonical engulfment proteins drive cell soma clearance, these are not required for process removal. We find that EFF-1, a protein previously implicated in cell–cell fusion[8], specifically promotes distal process phagocytosis. EFF-1 localizes to phagocyte pseudopod tips and acts exoplasmically to drive phagosome sealing. *eff-1* mutations result in phagocytosis arrest with unsealed phagosomes. Our studies suggest universal mechanisms for dismantling morphologically complex cells and uncover a phagosome-sealing component that promotes cell process clearance.

The *Caenorhabditis elegans* tail-spike cell (TSC) is a morphologically complex cell that extends a microtubule-laden process to the animal's tail tip. Wrapped around the TSC process is the hyp10 epithelial cell, which also extends posteriorly (Fig. 1a–d and Supplementary Fig. 1a). Ectopic TSC generation results in a forked tail[9] ($n=5$; Supplementary Fig. 1b,c), whereas early TSC ablation perturbs tail morphogenesis (five out of five ablated animals; Supplementary Fig. 1d,e). Thus, like hyp10, the TSC has a key role in *C. elegans* tail morphogenesis.

Once tail formation is complete, the TSC dies through transcriptional induction of the main *C. elegans* caspase, CED-3 (ref. [10]). By following myristoylated green fluroscent protein (GFP) expressed in the TSC, we found that a strong *ced-3* loss-of-function mutation promotes TSC soma and process persistence in larvae[10] (Fig. 1i and Supplementary Fig. 1d). However, only 30% of animals carrying a weak *ced-3* allele exhibit TSC persistence. Of these animals, 24% exhibit a fully intact cell, 30% have an intact cell soma alone and 18% exhibit an intact cell process alone. The remaining animals display TSCs at various states of degeneration (Fig. 1a–i). These observations demonstrate that CED-3 caspase drives cell process and cell soma degeneration independently.

To examine this idea more closely, we used myristoylated GFP to follow TSC death dynamics in 3-fold stage embryos by taking still images of different embryos at different time points ($n>50$). We find that degeneration begins with beading of the proximal cell process and rounding of the cell soma, followed by the appearance of a varicosity in the distal process. Clearance of the proximal process ensues, followed by distal process retraction into the distal varicosity (Fig. 1j–q). The TSC body and the distal varicosity are then engulfed and cleared by different neighbouring cells, with hyp10 engulfing the varicosity (see below). To confirm this event sequence, we imaged 14 individual animals over time using a custom-built inverted selective plane illumination microscope (iSPIM), which acquires rapid image volumes without motion-induced blurring[11]. We found the same sequence of events occurring over a period of about 170 minutes (Supplementary Video 1). Corroborating these results, serial-section transmission electron microscopy of a 3-fold embryo revealed proximal beading and distal varicosity formation (Fig. 1v and Supplementary Video 2). We also imaged a myristoylated mCherry reporter and obtained similar results (Supplementary Fig. 1f–i). Thus, independent morphological and molecular events dismantle the TSC soma, proximal process and distal process.

To determine whether similar degeneration dynamics occur in other morphologically complex cells, we examined the sex-specific CEMVL neuron that dies in hermaphrodites, but survive in males[12]. As embryonic CEMVL reporters are not known, we labelled the cells using our recently developed gene-induction system, in which CEMVL precursor cells, in animals carrying a heat-shock promoter::mCherry construct, are heated with an infrared laser for cell-specific labelling[13]. Time-lapse movies reveal that once generated, the CEMVL neuron extends a dendrite towards the nose tip. Dismantling of this axon-less neuron then occurs in a sequence resembling that of TSC dismantling ($n=6$; Fig. 1r–u and Supplementary Video 3). Thus, two different morphologically complex cell types use common spatially restricted programmes for death and clearance. Importantly, these studies also shed light on dendrite destruction, a phenomenon much less understood than axon degeneration[14].

We next wondered whether the compartment-specific clearance events we uncovered correspond to distinct molecular programmes. As imaging of CEMVL neurons is cumbersome, we pursued these studies in the TSC. We found that mutations affecting CED-1/Draper/MEGF10 and other apoptotic corpse engulfment regulators disrupt TSC soma clearance, with loss of CED-5/DOCK180 having the strongest effect[15,16] (Fig. 2a,b). However, single mutants in these genes, or a *ced-1;ced-5* double mutant have only minor defects in

[1]Laboratory of Developmental Genetics, The Rockefeller University, New York, NY, USA. [2]Developmental Biology Program, Sloan Kettering Institute, New York, NY, USA. [3]These authors contributed equally: Alina Rashid and Peter Insley. *e-mail: shaham@rockefeller.edu

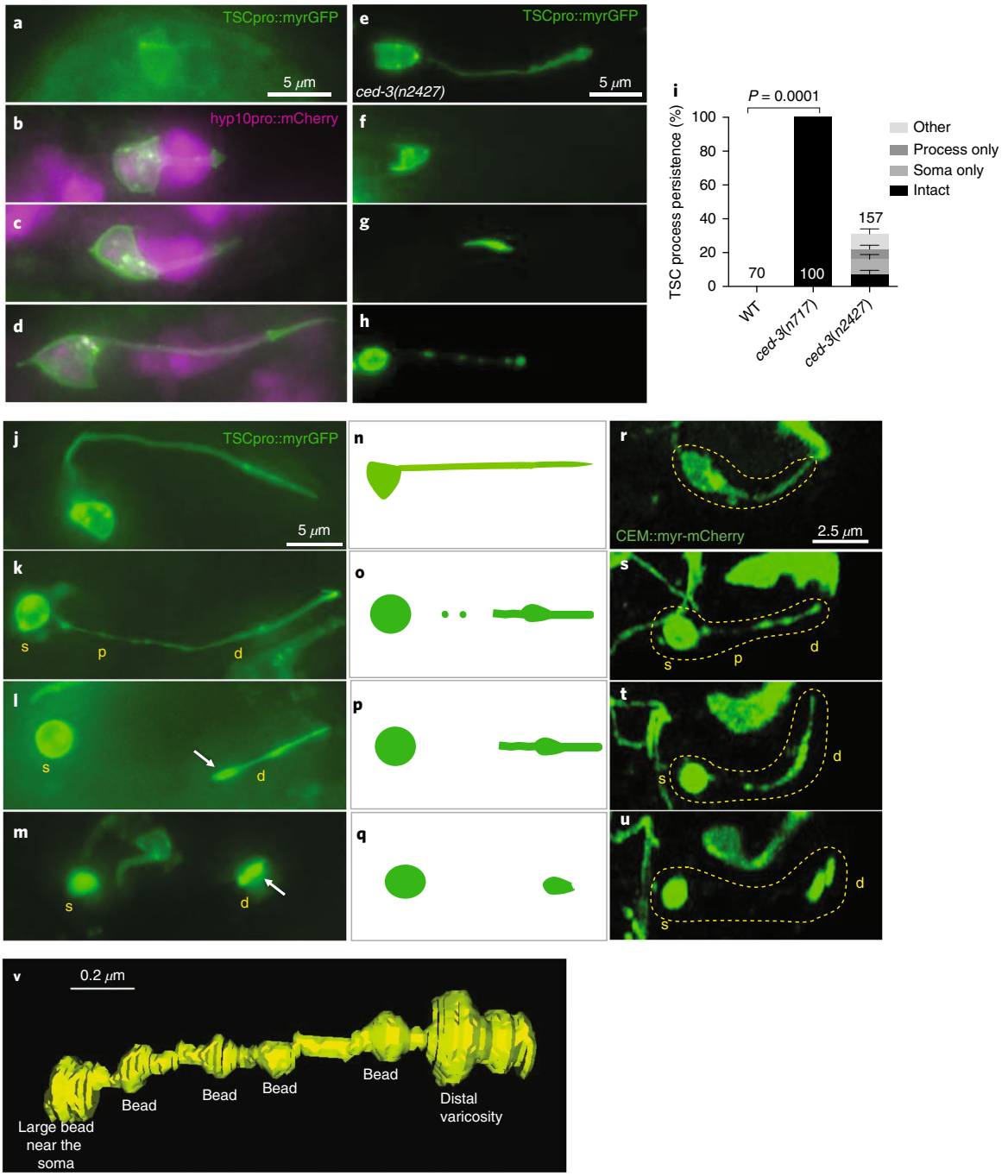

Fig. 1 | The TSC and CEM neurons undergo a similar degeneration sequence. a–d, TSC in the comma stage (**a**), 1.5-fold (**b**), 2-fold (**c**) and 3-fold (**d**) embryos and its association with hyp10. $n = 5$ biologically independent animals each with similar results. TSCpro, tail-spike cell promoter; myrGFP, myristoylated GFP. **e–h**, *ced-3(n2427)* mutants exhibit an intact cell (**e**), persistent soma only (**f**), persistent process only (**g**) or intermediate degeneration (other) (**h**). $n = 10$ biologically independent animals each with similar results. **i**, TSC persistence in *ced-3* mutants. Data are mean ± s.e.m. Statistics: two-tailed unpaired *t*-test. For individual *P* values, see Supplementary Table 2. Numbers inside/outside bars are the total animals scored per genotype. Data are from three independent scoring experiments. n = sample sizes for *ced-3(n2427)*: $n = 157$ (other: 42, process only: 31, soma only: 47, intact: 37). **j**, TSC in 3-fold embryo. **k**, TSC soma rounding and proximal process beading. **l**,**m**, Distal process varicocity (white arrow). $n = 10$ biologically independent animals each. **r–u**, Stills from movies showing CEM death. Yellow dashed line, cell outline. Time in hours:minutes post-fertilization: 07:40 (**r**), 08:05 (**s**), 08:15 (**t**) and 08:30 (**u**). **n–q**, Schematics for **j–m** and **r–u**. $n = 6$ biologically independent animals each. d, distal process; p, proximal process; s, soma. **v,** Three dimensional reconstruction of a degenerating TSC in an *eff-1(ns634)* animal. TSC death stages in this mutant are similar to WT (main text; Supplementary Video 5). Reconstruction is based on Supplementary Video 2. Statistics source data are provided in Supplementary Table 2.

proximal or distal process clearance (Fig. 2c). Mutations in *sand-1*/MON1, which is required for phagosome maturation[17], block cell soma and distal process clearance, but have no effects on proximal process elimination (Fig. 2d–f and Supplementary Video 4). These results suggest that distinct molecular programmes drive TSC soma, proximal process and distal process dismantling (Fig. 2g), and that

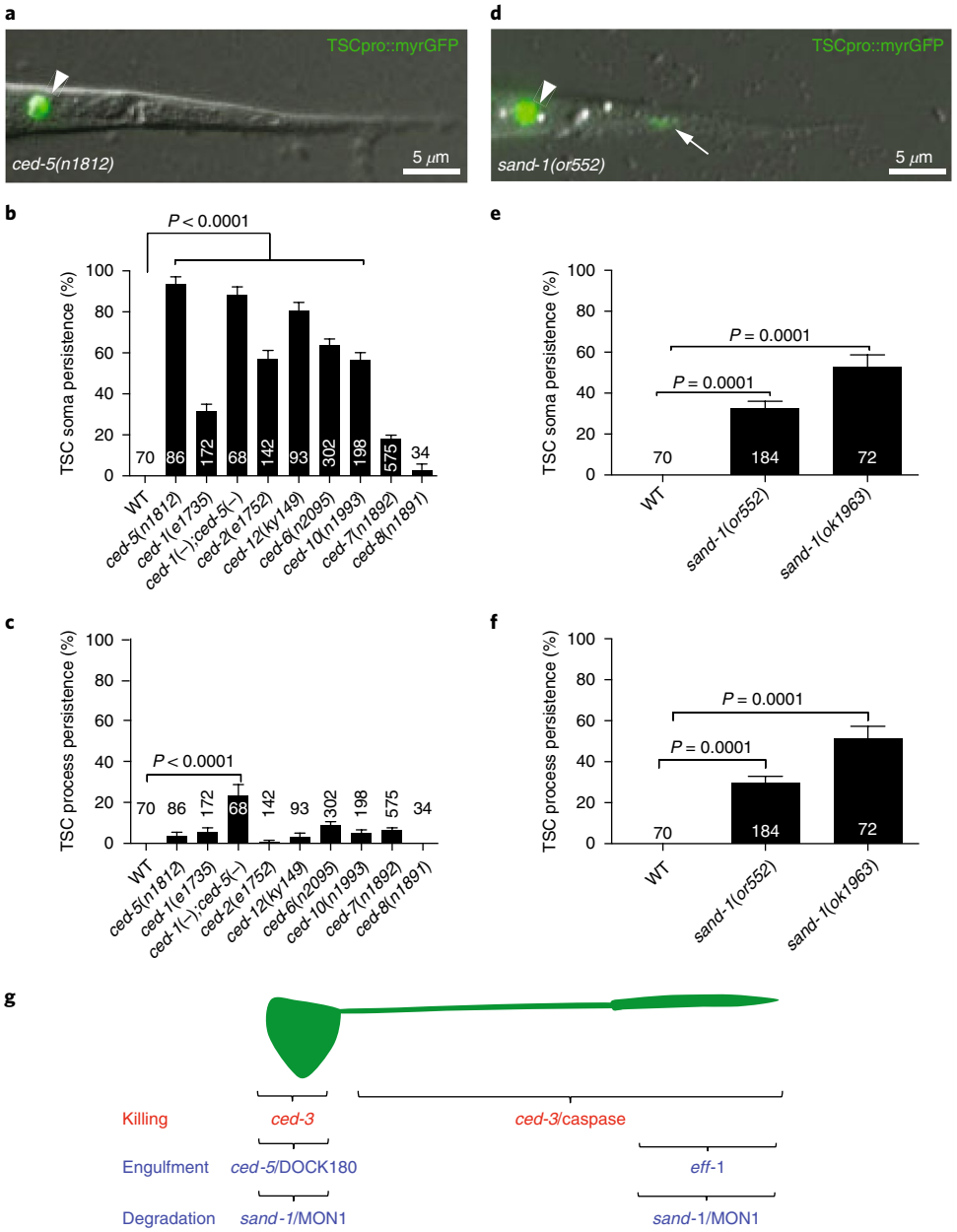

Fig. 2 | Canonical engulfment genes are not required for TSC process clearance. a, Unengulfed soma (arrowhead) in a *ced-5(n1812)* L1 animal. $n = 86$ biologically independent animals with similar results. **b**,**c**, TSC soma (**b**) and process (**c**) clearance defects. n = sample sizes for statistics, with the numbers inside/outside bars referring to the number of biologically independent animals. **d**, Undegraded soma and process in a *sand-1(or552)* L1 animal. Arrowhead indicates the soma; arrow indicates the process. $n = 184$ biologically independent animals with similar results. **e**,**f**, TSC soma (**e**) and process (**f**) degradation defects in *sand-1* mutants. n = sample sizes for statistics, with the numbers inside/outside bars referring to the number of biologically independent animals. **g**, Genes promoting TSC regional killing and clearance. Data in **b**,**c**,**e**,**f** are mean ± s.e.m. Statistics: two-tailed unpaired *t*-test. For individual *P* values, see Supplementary Table 2. Three independent scoring experiments were done. Statistics source data are provided in Supplementary Table 2.

additional genes promoting cell soma and process clearance remain to be identified.

To seek such genes, we mutagenized *C. elegans* expressing myristoyl-GFP in the TSC, and screened through ~27,000 F2 progeny for mutants with persisting TSC fragments. In addition to mutations in *ced-3*/caspase and *sand-1*/MON1, we isolated two mutants, *ns627* and *ns634*, that exhibit process clearance defects (Fig. 3a,b) but do not affect soma removal ($n > 100$ each). Mutant L1 larvae do not exhibit other persistent cell corpses seen in apoptotic engulfment mutants[18] ($n > 70$).

Using whole-genome sequencing, single-nucleotide polymorphism mapping and transformation rescue, we demonstrated that both mutants harbour causal lesions in the gene *eff-1*, which encodes a transmembrane protein with structural homology to viral class II fusion proteins, that promote cell–cell fusion[8]. Confirming this, animals homozygous for the canonical *eff-1(hy21)* allele also exhibit TSC clearance defects (Fig. 3b). Both mutants we isolated have animal morphology defects resembling those of *eff-1(hy21)* mutants, suggesting that they also lack cell fusion events. Consistent with this, both alleles perturb the EFF-1 extracellular domain (Fig. 3c).

To determine which part of the TSC process persists in *eff-1* mutants, we imaged TSC death using iSPIM. Although cell soma degradation, proximal process degradation and distal process

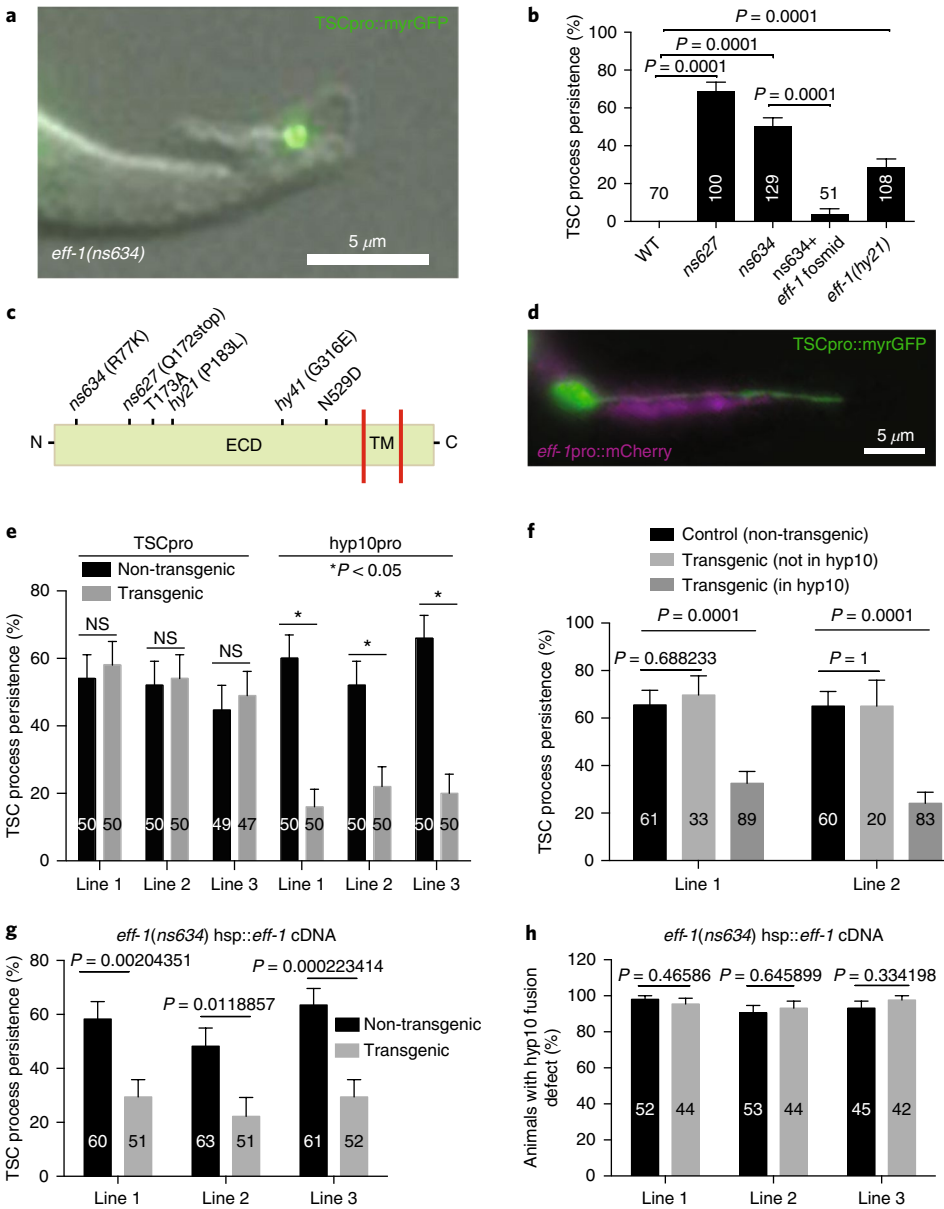

Fig. 3 | EFF-1 fusogen mediates distal process clearance. a, L1 *eff-1(ns634)* mutant. $n = 129$ biologically independent animals with similar results. **b**, Process clearance defects in the indicated genotypes. n = sample sizes for statistics, with the numbers inside/outside bars referring to the number of biologically independent animals. **c**, EFF-1 structure and mutation sites. ECD, extracellular domain; TM, transmembrane domain. *hy41* was previously identified[14]. **d**, *ced-3(n717)* mutant showing hyp10 *eff-1* expression. $n = 4$ biologically independent animals with similar results. **e**, *eff-1*-mutant cell-specific rescue. n = sample sizes for statistics, with the numbers inside bars referring to the number of biologically independent animals. **f**, Mosaic analysis showing EFF-1 function in hyp10 for TSC distal process clearance. n = sample sizes for statistics. **g**, Rescue of *eff-1*-mutant TSC clearance defect with heat-shock promoter (hsp)::*eff-1* cDNA following heat exposure. n = sample sizes. **h**, Same as **g**, except rescue of fusion was examined. n = sample sizes. Data in **b**,**e**–**h** are mean ± s.e.m. Statistics: two-tailed unpaired *t*-test. NS, not significant ($P > 0.05$). For individual *P* values, see Supplementary Table 2. For rescue experiments, 2–3 independent transgenic lines were scored. For other experiments, three independent scoring experiments were done. For heat-shock rescue, scoring was done 2 hours after heat shock. Statistics source data are provided in Supplementary Table 2.

retraction were unaffected, distal process varicosity clearance was blocked (Supplementary Video 5).

To determine where EFF-1 functions, we first examined its expression pattern. In *ced-3(n717)*-mutant larvae, in which a live TSC persists, an *eff-1* promoter::mCherry reporter is expressed in hyp10, but not in the TSC (Fig. 3d). Thus, EFF-1 probably functions in the engulfing cell. Supporting this, expression of an *eff-1* complementary DNA using a TSC-specific promoter fails to rescue distal process clearance defects of *eff-1* mutants; however, expression of the same cDNA using a hyp10-expressed *eff-1* promoter fragment rescues these defects (Fig. 3e). Furthermore, in animals carrying an unstable extrachromosomal array containing the *eff-1* locus, array presence/absence in hyp10 strongly correlates with distal fragment clearance/persistence (Fig. 3f). Thus, EFF-1 functions in the hyp10 engulfing cell for TSC distal process clearance (Fig. 2g).

During embryogenesis, two hyp10 cells fuse to form the hyp10 syncytium, which engulfs the TSC distal process. As EFF-1 controls cell fusion, distal process clearance defects in *eff-1* mutants may reflect hyp10 cell–cell fusion failure. Arguing against this, however, *eff-1* mutants have fully penetrant tail morphology defects,

probably resulting from cell–cell fusion defects; yet, we found rare *eff-1(ns634);*hyp10p::*eff-1* animals in which tail-tip defects were rescued but distal process engulfment still failed, suggesting that hyp10 cell–cell fusion and distal fragment clearance are separable events. To test this directly, we followed hyp10 cell–cell fusion using the AJM-1::GFP reporter, labelling junctions between unfused cells[19]. One-hundred per cent of *eff-1*-mutant animals exhibit hyp10 cell–cell fusion defects; however, only 40% have TSC clearance defects ($n=48$) (Supplementary Fig. 2b,c). Thus, blocking hyp10 cell–cell fusion is not sufficient to block distal process engulfment. To further address this issue, we subjected *eff-1(ns634)* mutants, which carry heat-inducible *eff-1* cDNA transgenes, to elevated temperatures and assessed distal process clearance and hyp10 cell–cell fusion. Although distal fragments were cleared within 2 hours of heat exposure, cell fusion was restored more slowly (Fig. 3g,h), beginning only 4–6 hours later. Together, these studies suggest that hyp10 cell–cell fusion defects alone cannot explain TSC distal fragment clearance failure. Thus, *eff-1* probably has direct roles in distal process clearance.

EFF-1 could be required for distal process varicosity recognition by hyp10, phagosome sealing, phagosome maturation or lysosomal degradation. We found that the varicosity is usually surrounded by hyp10 pseudopods in *eff-1* mutants; however, gaps are often seen in optical cross-sections (Fig. 4a and Supplementary Video 6), suggesting that, although the varicosity is being recognized, it is not fully internalized. Electron micrographs of an *eff-1(ns634)* mutant support the idea that phagosome sealing is defective in *eff-1* mutants (Fig. 4b).

To confirm these results, we examined the localization of phagosome-associated proteins around the distal fragment remnant. We found that hyp10-expressed mKate2 fluorescent protein fused to the pleckstrin homology (PH) domain of phospholipase C-δ, which marks unsealed phagosomes[20], is enriched around the TSC distal process varicosity (eight out of eight animals; Fig. 4c and Supplementary Video 7). The closed phagosome marker GFP::2xFYVE[20] is generally not enriched (19 out of 20 animals; Supplementary Fig. 3a–c and Supplementary Video 8). A marker for mature phagosomes, RAB-7 (ref. [21]), also does not localize around the distal process remnant (Supplementary Fig. 3d–f and Supplementary Video 9), nor does LAAT-1::mCherry, a phagolysosome marker[20] (Supplementary Fig. 3g–i and Supplementary Video 10). Thus, the distal process fragment resides in an unsealed phagosome.

To directly test whether the distal process phagosome is open in *eff-1* mutants, we reasoned that its interior should be continuous with the extracellular milieu. A fluorescent molecule expressed in this milieu should penetrate the phagosome only if the organelle is open (Supplementary Fig. 4e,f). Thus, we generated *eff-1(ns634);cup-2(ar506)* mutants expressing secreted GFP (ssGFP) from body muscle using the *myo-3* promoter[22]. In wild-type (WT) animals, ssGFP is taken up by coelomocyte scavenger cells; however, *cup-2(ar506)* blocks this uptake, allowing ssGFP extracellular accumulation. *cup-2(ar506)* mutants do not have TSC clearance defects ($n=10$). Most *eff-1(ns634);cup-2(ar506); myo-3*p::ssGFP animals exhibit GFP fluorescence between the phagosome membrane and the TSC remnant, suggesting access to the phagosome at some point in time (Fig. 4d, Supplementary Fig. 4a–d and Supplementary Video 11). We photobleached the signal surrounding the TSC remnant and assessed whether fluorescence recovered (Supplementary Fig. 4). Signal recovery occurred over a period of 5 seconds (19 animals) to 30 minutes (11 animals) in most animals observed ($n=38$; Fig. 4d–f and Supplementary Videos 12,13), strongly supporting the notion that the mutant phagosome is unsealed. We speculate that fluorescence recovery time may correlate with phagosome gap size. As a control, we looked at *sand-1(or522);cup-2(ar506)* mutants ($n=45$), in which a sealed, persisting phagosome is expected. Forty-four animals had no GFP accumulation around the TSC, probably because phagosomes were sealed before ssGFP expression. One animal exhibited GFP accumulation (Supplementary Fig. 4g–r and Supplementary Video 14), but GFP fluorescence did not recover following photobleaching, suggesting that the phagosome is closed (Supplementary Fig. 4f).

Several *C. elegans* proteins are implicated in phagosome sealing, including MTM-1/myotubularin, OCRL-1/inositol 5-phosphatase, LST-4/SNX9, PIKI-1/PI3K and DYN-1/dynamin[20]. Dynamin proteins also have roles in intracellular scission of endocytic vesicles, although dynamin-independent endocytosis has been documented[23]. However, mutants in these genes have no effect on distal process removal (Supplementary Table 1). We also examined DYN-1::GFP localization using iSPIM in WT animals ($n=3$ movies). Although DYN-1::GFP enrichment was seen around the cell soma, enrichment was not observed around the distal process fragment. Thus, phagosome sealing during distal process engulfment may be independent of known sealing components.

EFF-1 roles in cell fusion have been extensively characterized. Like viral fusion proteins, the expression of EFF-1 alone is sufficient for cell–cell fusion in heterologous systems[24], which suggests that it drives membrane rearrangements without additional proteins. Such an independent function could explain why the standard phagosome-sealing machinery is dispensable for TSC distal process clearance. We noted that *eff-1(ns634)* mutants, which contain an R77K mutation in the EFF-1 extracellular domain, are cell-fusion defective (Fig. 3h). Furthermore, EFF-1(R77K) protein localizes to the plasma membrane and vesicular structures (Supplementary Fig. 2d), like WT EFF-1. Thus, EFF-1 fusogenic function seems to be required for phagosome sealing. Supporting this notion, neither EFF-1(R77K) nor EFF-1(G316E) (which is also fusion defective and properly localized; B. Podbilewicz, personal communication) rescue the distal process clearance defect of *eff-1(ns634)* mutants (Fig. 4h and Supplementary Fig. 2a).

If indeed EFF-1 promotes phagosome sealing through autocellular fusion, we would expect the protein to localize to the convergence site of phagosome arms. To test this, we examined the localization of the EFF-1(T173A;N529D)::GFP fusion-defective protein, which shows proper localization in other contexts[25,26], in an *eff-1(ns634)* mutant. In 14 out of 15 animals, EFF-1 localized at the TSC remnant. Strikingly, in animals where a phagosome opening was seen, EFF-1 localized to phagosome arm tips (five out of five; Fig. 4i–l and Supplementary Video 15), supporting the notion that EFF-1 promotes phagosome sealing through autocellular fusion.

We demonstrate here that different morphologically complex cell types, an epithelial cell and a neuron, undergo similar events dismantling and clearing their cell soma and processes. That two disparate *C. elegans* cell types are similarly eliminated raises the possibility that neurons and other morphologically complex cells are removed by related mechanisms across animals.

Different programmes seem to promote degeneration of distinct cellular domains, and dismantling initiation of each domain proceeds independently of the others. Cell somas undergo morphological changes resembling apoptosis and require canonical apoptotic engulfment genes for clearance. Proximal processes undergo caspase-dependent fragmentation and beading, reminiscent of Wallerian degeneration. However, mutations in genes required for Wallerian degeneration in *Drosophila* and in mice, and for linker cell-type death (LCD) in *C. elegans*, do not block TSC proximal process degeneration and clearance[6,27] (*tir-1*/Sarm or *btbd-2*; Supplementary Table 1), suggesting that an alternative molecular programme may underlie this form of degeneration. Distal processes undergo retraction into a varicosity.

Separate clearance mechanisms also drive compartment removal, and we identify a key player, EFF-1/fusogen, that is required for the clearance of the distal process varicosity. Sealing of phagosomes and endocytic vesicles has been proposed to occur through the action of the protein dynamin[28], or in the case of dynamin-independent

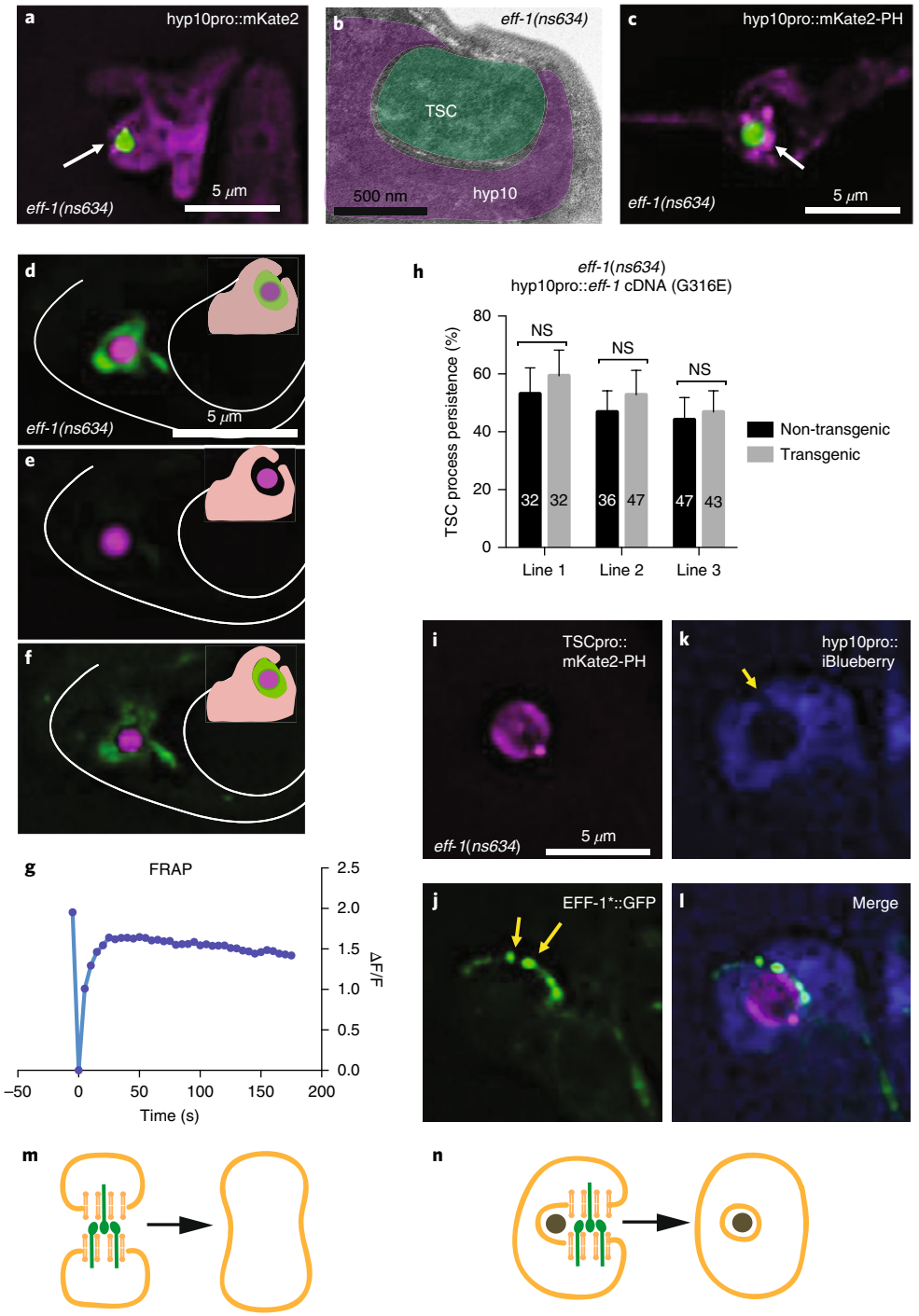

Fig. 4 | EFF-1 promotes phagosome sealing. a, The TSC distal process is incompletely engulfed by the hyp10 cell. The arrow indicates the phagosome opening. $n=15$ biologically independent animals with similar results. **b**, Electron micrograph of *eff-1(ns634)* L1 showing an open phagosome. The area that is not pseudocoloured indicates the cuticle. $n=1$ animal. **c**, Enrichment of the open phagosome marker (arrow) around the TSC fragment. $n=10$ biologically independent animals with similar results. **d**–**f**, FRAP experiment in *eff-1(ns634) cup-2(ar506)*. ssGFP, secreted GFP, is green; TSC is in magenta. The TSC is shown in the inset, with secreted GFP in the phagosome space, before (**d**), immediately after (**e**), and 30 min after photobleaching (**f**). $n=11$ biologically independent animals with similar results. **g**, Quantification of a different FRAP experiment. $n=19$ biologically independent animals with similar results. **h**, EFF-1(G316E) cannot rescue *eff-1(ns634)* distal fragment clearance defect. $n=$ sample sizes for statistics, with the numbers inside bars indicating the total animals scored per genotype. Data are mean ± s.e.m. Statistics: two-tailed unpaired *t*-test. For individual *P* values, see Supplementary Table 2. NS, not significant ($P>0.05$). **i**–**l**, Localization of EFF-1 (arrows in **j**) at phagosome arm tips (arrow in **k**). $n=4$ biologically independent animals with similar results. **m**,**n**, Models of EFF-1 (green) function in cell–cell fusion (**m**) and phagosome sealing (**n**). Three independent transgenic lines were scored for the rescue experiment. FRAP experiments were repeated 38 times.

endocytosis, through bar-domain proteins[29]. Nonetheless, whether these factors are directly responsible for membrane fusion is debated. Unlike previously described membrane-scission factors, EFF-1 acts exoplasmically. Our studies are consistent with a model in which EFF-1 promotes autocellular fusion to generate a sealed phagosome in much the same way it promotes fusion of two cells (Fig. 4m,n).

Such EFF-1-mediated autocellular fusion is also proposed in axonal regeneration[30,31], dendrite sculpting[14,32] and in single-cell tube formation[33]. EFF-1 is necessary and sufficient to drive cell fusion[34] and could similarly be the only factor required for phagosome sealing.

Recently, an EFF-1-related protein, HAP2, was found to promote gamete fusion across several phyla[35]. As EFF-1, HAP2 and class II fusogens share limited sequence similarity, it is possible that yet uncharacterized but structurally related proteins in other eukaryotes also promote phagosome sealing.

Methods

Methods, including statements of data availability and any associated accession codes and references, are available at https://doi.org/10.1038/s41556-018-0068-5.

Received: 8 August 2017; Accepted: 16 February 2018;
Published online: 19 March 2018

References

1. Lekstrom-Himes, J. A. & Gallin, J. I. Immunodeficiency diseases caused by defects in phagocytes. *N. Engl. J. Med.* **343**, 1703–1714 (2000).
2. Levin, R., Grinstein, S. & Canton, J. The life cycle of phagosomes: formation, maturation, and resolution. *Immunol. Rev.* **273**, 156–179 (2016).
3. Mallat, M., Marin-Teva, J. L. & Cheret, C. Phagocytosis in the developing CNS: more than clearing the corpses. *Curr. Opin. Neurobiol.* **15**, 101–107 (2005).
4. Hochreiter-Hufford, A. & Ravichandran, K. S. Clearing the dead: apoptotic cell sensing, recognition, engulfment, and digestion. *Cold Spring Harb. Perspect. Biol.* **5**, a008748 (2013).
5. Reddien, P. W. & Horvitz, H. R. The engulfment process of programmed cell death in *Caenorhabditis elegans*. *Annu. Rev. Cell Dev. Biol.* **20**, 193–221 (2004).
6. Osterloh, J. M. et al. dSarm/Sarm1 is required for activation of an injury-induced axon death pathway. *Science* **337**, 481–484 (2012).
7. Simon, D. J. et al. Axon degeneration gated by retrograde activation of somatic pro-apoptotic signaling. *Cell* **164**, 1031–1045 (2016).
8. Mohler, W. A. et al. The type I membrane protein EFF-1 is essential for developmental cell fusion. *Dev. Cell* **2**, 355–362 (2002).
9. Chiorazzi, M. et al. Related F-box proteins control cell death in *Caenorhabditis elegans* and human lymphoma. *Proc. Natl Acad. Sci. USA* **110**, 3943–3948 (2013).
10. Maurer, C. W., Chiorazzi, M. & Shaham, S. Timing of the onset of a developmental cell death is controlled by transcriptional induction of the *C. elegans ced-3* caspase-encoding gene. *Development* **134**, 1357–1368 (2007).
11. Wu, Y. et al. Inverted selective plane illumination microscopy (iSPIM) enables coupled cell identity lineaging and neurodevelopmental imaging in *Caenorhabditis elegans*. *Proc. Natl Acad. Sci. USA* **108**, 17708–17713 (2011).
12. Nehme, R. et al. Transcriptional upregulation of both *egl-1* BH3-only and *ced-3* caspase is required for the death of the male-specific CEM neurons. *Cell Death Differ.* **17**, 1266–1276 (2010).
13. Singhal, A. & Shaham, S. Infrared laser-induced gene expression for tracking development and function of single *C. elegans* embryonic neurons. *Nat. Commun.* **8**, 14100 (2017).
14. Oren-Suissa, M., Hall, D. H., Treinin, M., Shemer, G. & Podbilewicz, B. The fusogen EFF-1 controls sculpting of mechanosensory dendrites. *Science* **328**, 1285–1288 (2010).
15. Wu, Y. C. & Horvitz, H. R. *C. elegans* phagocytosis and cell-migration protein CED-5 is similar to human DOCK180. *Nature* **392**, 501–504 (1998).
16. Zhou, Z., Hartwieg, E. & Horvitz, H. R. CED-1 is a transmembrane receptor that mediates cell corpse engulfment in *C. elegans*. *Cell* **104**, 43–56 (2001).
17. Kinchen, J. M. & Ravichandran, K. S. Identification of two evolutionarily conserved genes regulating processing of engulfed apoptotic cells. *Nature* **464**, 778–782 (2010).
18. Ellis, R. E., Jacobson, D. M. & Horvitz, H. R. Genes required for the engulfment of cell corpses during programmed cell death in *Caenorhabditis elegans*. *Genetics* **129**, 79–94 (1991).
19. Koppen, M. et al. Cooperative regulation of AJM-1 controls junctional integrity in *Caenorhabditis elegans* epithelia. *Nat. Cell Biol.* **3**, 983–991 (2001).
20. Cheng, S. et al. PtdIns(4,5)P(2) and PtdIns3P coordinate to regulate phagosomal sealing for apoptotic cell clearance. *J. Cell Biol.* **210**, 485–502 (2015).
21. Guo, P., Hu, T., Zhang, J., Jiang, S. & Wang, X. Sequential action of *Caenorhabditis elegans* Rab GTPases regulates phagolysosome formation during apoptotic cell degradation. *Proc. Natl Acad. Sci. USA* **107**, 18016–18021 (2010).
22. Fares, H. & Greenwald, I. Genetic analysis of endocytosis in *Caenorhabditis elegans*: coelomocyte uptake defective mutants. *Genetics* **159**, 133–145 (2001).
23. Kumari, S. & Mayor, S. ARF1 is directly involved in dynamin-independent endocytosis. *Nat. Cell Biol.* **10**, 30–41 (2008).
24. Podbilewicz, B. et al. The *C. elegans* developmental fusogen EFF-1 mediates homotypic fusion in heterologous cells and in vivo. *Dev. Cell* **11**, 471–481 (2006).
25. del Campo, J. J. et al. Fusogenic activity of EFF-1 is regulated via dynamic localization in fusing somatic cells of *C. elegans*. *Curr. Biol.* **15**, 413–423 (2005).
26. Smurova, K. & Podbilewicz, B. Endocytosis regulates membrane localization and function of the fusogen EFF-1. *Small GTPases* **8**, 177–180 (2017).
27. Kinet, M. J. et al. HSF-1 activates the ubiquitin proteasome system to promote non-apoptotic developmental cell death in *C. elegans*. *eLife* **5**, e12821 (2016).
28. van der Bliek, A. M. & Meyerowitz, E. M. Dynamin-like protein encoded by the *Drosophila shibire* gene associated with vesicular traffic. *Nature* **351**, 411–414 (1991).
29. Simunovic, M. et al. Friction mediates scission of tubular membranes scaffolded by BAR proteins. *Cell* **170**, 172–184.e11 (2017).
30. Neumann, B. et al. EFF-1-mediated regenerative axonal fusion requires components of the apoptotic pathway. *Nature* **517**, 219–222 (2015).
31. Ghosh-Roy, A., Wu, Z., Goncharov, A., Jin, Y. & Chisholm, A. D. Calcium and cyclic AMP promote axonal regeneration in *Caenorhabditis elegans* and require DLK-1 kinase. *J. Neurosci.* **30**, 3175–3183 (2010).
32. Oren-Suissa, M., Gattegno, T., Kravtsov, V. & Podbilewicz, B. Extrinsic repair of injured dendrites as a paradigm for regeneration by fusion in *Caenorhabditis elegans*. *Genetics* **206**, 215–230 (2017).
33. Rasmussen, J. P., English, K., Tenlen, J. R. & Priess, J. R. Notch signaling and morphogenesis of single-cell tubes in the *C. elegans* digestive tract. *Dev. Cell* **14**, 559–569 (2008).
34. Shemer, G. et al. EFF-1 is sufficient to initiate and execute tissue-specific cell fusion in *C. elegans*. *Curr. Biol.* **14**, 1587–1591 (2004).
35. Fedry, J. et al. The ancient gamete fusogen HAP2 is a eukaryotic class II fusion protein. *Cell* **168**, 904–915 (2017).

Acknowledgements

We thank members of the Shaham lab for discussions and critical comments on the manuscript. We thank F. Soulavie and M. Sundaram for sharing data. Some strains were provided by the CGC, which is funded by the NIH Office of Research Infrastructure Programs (P40 OD010440) and the National Bioresource Project of Japan. The work was supported by a Rockefeller Women and Science Fellowship and the NIH grant 1F32HD089640 to P.G. and by NIH grants R01NS081490 and R01NS078703 to S.S.

Author contributions

P.G. and S.S. wrote the manuscript and analysed the results. A.R. and P.I. performed the iSPIM imaging. A.S. and A.R. performed the CEM imaging. M.T. helped map the mutants. P.S. and Z.B. performed the TSC ablations. Y.L. performed the electron microscopy. P.G. performed all other experiments.

Competing interests

The authors declare no competing interests.

Additional information

Supplementary information is available for this paper at https://doi.org/10.1038/s41556-018-0068-5.

Reprints and permissions information is available at www.nature.com/reprints.

Correspondence and requests for materials should be addressed to S.S.

Publisher's note: Springer Nature remains neutral with regard to jurisdictional claims in published maps and institutional affiliations.

Methods

***C. elegans* methods.** *C. elegans* strains were cultured using standard methods[36] and were grown at 20 °C. WT animals were the Bristol N2 subspecies. For most TSC experiments, one of three integrated reporters were used: *nsIs435*, *nsIs528* or *nsIs685*. Integration of extrachromosomal arrays was performed using UV and trioxalen (T2137, Sigma). For most experiments, animals were scored at 20 °C, with the exception of the *ced-3* experiment, which was done at 25 °C.

Mutants. The list of mutant *C. elegans* strains used in this study is as follows:
LGI: *ced-1(e1735)*, *ced-1(n2089)*, *cup-2(ar506)*, *ced-12(ky149)*
LGII: *eff-1(hy21)*, *aff-1(tm2214)*
LGIII: *ced-6(n2095)*, *ced-7(n1982)*, *tir-1(qd4)*
LGIV: *ced-3(n717)*, *ced-3(n2427)*, *ced-5(n1812)*, *ced-2(e1752)*, *ced-10(n1993)*, *sand-1(or522)*, *sand-1(ok1963)*, *lst-4(tm2423)*, *tag-30/btbd-2(gk474281)*
LGX: *ced-8(n1891)*, *dyn-1(ky51)*, *piki-1(ok2346)*

Germline transformation and rescue experiments. Germline transformation was carried out as previously described[37]. All plasmids were injected at between 1 and 20 ng per µl. pUC19 was used to adjust the DNA concentration of injection mixtures if necessary. All rescue experiments were done with *myo-2*p::GFP as a co-injection marker along with *cdh-3*p::mCherry to label hyp10 and TSC.

Transgenes. The full list of transgenes is described in Supplementary Table 4. The full length or fragment of the *aff-1* promoter was used to label the TSC. To label hyp10, either the *cdh-3* promoter (embryo imaging only) or the *eff-1* promoter (all other experiments) was used.

Primers and plasmid construction. Primer sequences and information on the construction of plasmids used in this study are provided in Supplementary Table 3.

Scoring of TSC. TSC death was scored at the L1 stage. Animals were synchronized by treating gravid hermaphrodites with alkaline bleach and allowing the eggs to hatch in M9 medium overnight. Synchronized L1s were then mounted on slides on 2% agarose-water pads, anaesthetized in 10 mM sodium azide and examined on a Zeiss Axioplan 2 or Axio-Scope A1 under Nomarski optics and wide-field fluorescence at ×40. The TSC was identified by green fluorescence (from reporter transgenes) as well as by its location and morphology.

Mutagenesis and mutant identification. *nsIs435* animals were mutagenized using 75 mM ethylmethanesulfonate (M0880, Sigma) for 4 h at 20 °C. Approximately 27,000 F2 progeny were screened for TSC persistence on a Zeiss Axio-Scope A1 at ×40. *eff-1(ns634)* and *eff-1(ns627)* were mapped to segment 9 of chromosome II by Hawaiian single nucleotide polymorphism (SNP) mapping[38]. The gene was identified by fosmid rescue and candidate gene analysis. See Supplementary Table 5.

Quantification of apoptotic cell corpse persistence. General engulfment defects were scored as persistent corpses in the heads of L1 larvae that were anaesthetized with 30 mM sodium azide and mounted on agar pads, using Nomarski optics. $n = 70$ for WT and $n = 78$ for *eff-1(ns634)*.

Mosaic analysis. Three lines of *eff-1(ns634)*TSC::myrGFP animals with unstable extrachromosomal arrays of *eff-1*p::*eff-1* cDNA-SL2-myr-mCherry were studied. Animals that either had mCherry (and hence *eff-1*) expression in hyp10, or that did not have expression, were scored for a TSC defect. Non-transgenic animals were used as controls.

Scoring cell fusion. The apical junctional marker AJM-1::GFP was used to score cell fusion defects indicated by the presence of a AJM-1::GFP-labelled membrane. We define fusion as the loss of AJM-1::GFP from junctions[34].

Heat-shock experiments. Transgenic animals carrying a heat-inducible *hsp-16.2* promoter driving *eff-1* cDNA and an SL2 myristoylated mCherry were generated. These animals and siblings without the array at the synchronized L1 stage were heat-shocked in a water bath at 33 °C and allowed to recover at 20 °C for 2 h in liquid (M9) culture. Animals were then scored for either TSC process persistence or hyp10 fusion (AJM-1::GFP) on slides.

Electron microscopy. *eff-1(ns634) nsIs435* L1 larvae were imaged using a Zeiss Axioplan 2 compound microscope to measure the relative location of the TSC within the worm relative to the tail tip using the AxioVision software (Zeiss). Animals were then fixed, stained, embedded in resin and sectioned using standard methods[39]. Images were acquired on an FEI TECNAI G2 Spirit BioTwin transmission electron microscope with a Gatan 4 K × 4 K digital camera at The Rockefeller University Electron Microscopy Resource Center.

Microscopy and image processing. Some images were collected on an Axioplan 2 microscope (Zeiss) with ×63/1.4 numerical aperture (NA) objective (Zeiss) and dual-band filter set (set 51019, Chroma). Most images were collected on a DeltaVision Core imaging system at the Rockefeller Bioimaging Facility (GE Healthcare Life Sciences) with an Olympus IX-71 microscope and Insight 7 colour SSI illumination system using an UPLSAPO ×60/1.3 NA silicone oil objective (Olympus) and a pro.edge sCMOS camera. Images were acquired and deconvolved using measured point-spread functions using SoftWorx software (GE Healthcare Life Sciences). For still embryo imaging, embryos were anaesthetized using 0.5 M sodium azide. Larvae were paralysed as described above.

Fluorescence recovery after photobleaching. Fluorescence recovery after photobleaching (FRAP) experiments were performed on a DeltaVision Core imaging system at the Rockefeller Bioimaging Facility using the 410, 488 and 532 laser module (QLM). Live L1 larvae were mounted and immobilized using 10 mM sodium azide. GFP surrounding the TSC was selectively photobleached at 25% 406-nm laser power for a 0.250-second pulse. Post-bleach images were collected at 5-second intervals for 3 min. Some animals showed GFP recovery later and were imaged 30 min after photobleaching.

Scoring CEM neurons. CEM examination was done following a previous study[16]. Embryos were mounted using 20-mm bead spacers or 2% agarose pads. During heat-shock induction, the cell was irradiated for five continuous minutes. Precursor cells were identified using a nuclear UNC-130-GFP marker. When four cells were labelled and the signal co-localized with UNC-130-GFP, induction was scored as specific.

iSPIM imaging. Light-sheet microscope imaging was performed on a custom-built iSPIM based on a previously published design[11] using a Hammamatsu Orca Flash 4.0 camera. Embryos that were collected by dissecting gravid adults were mounted on a coverslip with a polylysine solution (Sigma) spot. Imaging conditions were as follows: temperature: 20–22 °C; laser power (488-nm solid state laser): 100–130 µW; exposure time: 10.2–20 ms; and time between stacks: 2–3 min.

TSC ablation. Embryonic ablations were performed using an Olympus UPLSAPO ×60 objective on a Zeiss AxioObserver Z1 frame equipped with a Yokogawa CSU-X1 spinning disk head and two Hamamatsu C9100-13 EM-CCD cameras. Ablations were performed on *ced-3(n717)* embryos to verify successful ablation. Embryos at the 2-cell or 4-cell stage were cut from gravid hermaphrodites and mounted based on standard protocols[40]. TSC precursors were identified by tracing the embryonic lineage up until their terminal division. A total of 35 low-energy pulses were delivered at 2 Hz to each of the TSC precursors 7 min after observing the beginning of each cell's cytokinesis. The ablated TSC precursors and their hyp10 siblings were then tracked to verify that the TSC precursors died and were extruded from the embryo while the hyp10 cells migrated to their correct final position and showed no signs of damage. Embryos in which one or more TSC precursors failed to be extruded or in which off-target damage was observed in neighbouring cells were burst using a high-energy laser pulse. The embryos were allowed to hatch overnight before the resulting larvae were recovered and mounted for imaging.

Statistics and reproducibility. The samples sizes and statistical tests were selected based on previous studies with similar methodologies. Sample sizes were not determined using statistical methods. All experiments were repeated at least two to three times, as indicated, giving similar results. Independent transgenic lines were treated as independent experiments. Quantification of TSC persistence was done using an unpaired two-tailed *t*-test (Graphpad). For all figures, mean ± standard error of the mean (s.e.m.) is represented. For Fig. 4b, $n = 1$, Supplementary Fig. 1a, $n = 1$; Supplementary Fig. 1b, $n = 2$, Supplementary Fig. 1f–i, $n = 2$ and Supplementary Fig. 4g–r, $n = 1$, where $n =$ the number of biologically independent animals. Source data for Figs. 1a–h,j,m,r,u,v, 2a,d, 3a,d and 4a–g and Supplementary Figs. 1a–i, 2b–d, 3a–i and 4a–d,g–r can be found in Supplementary Table 2.

Life Sciences Reporting Summary. Further information on experimental design is available in the Life Sciences Reporting Summary.

Data availability. Source data for Figs. 1–4 and Supplementary Fig. 2 have been provided as Supplementary Table 2. All other data supporting the findings of this study are available from the corresponding author on reasonable request.

References

36. Brenner, S. The genetics of *Caenorhabditis elegans*. *Genetics* **77**, 71–94 (1974).
37. Mello, C. C., Kramer, J. M., Stinchcomb, D. & Ambros, V. Efficient gene transfer in *C.elegans*: extrachromosomal maintenance and integration of transforming sequences. *EMBO J.* **10**, 3959–3970 (1991).
38. Wicks, S. R., Yeh, R. T., Gish, W. R., Waterston, R. H. & Plasterk, R. H. Rapid gene mapping in *Caenorhabditis elegans* using a high density polymorphism map. *Nat. Genet.* **28**, 160–164 (2001).
39. Lundquist, E. A., Reddien, P. W., Hartwieg, E., Horvitz, H. R. & Bargmann, C. I. Three *C. elegans* Rac proteins and several alternative Rac regulators control axon guidance, cell migration and apoptotic cell phagocytosis. *Development* **128**, 4475–4488 (2001).
40. Bao, Z. & Murray, J. I. Mounting *Caenorhabditis elegans* embryos for live imaging of embryogenesis. *Cold Spring Harb. Protoc.* **2011**, prot065599 (2011).

nature research

Corresponding Author: Shai Shaham

Date: Dec 21, 2017

Life Sciences Reporting Summary

Nature Research wishes to improve the reproducibility of the work we publish. This form is published with all life science papers and is intended to promote consistency and transparency in reporting. All life sciences submissions use this form; while some list items might not apply to an individual manuscript, all fields must be completed for clarity.

For further information on the points included in this form, see Reporting Life Sciences Research. For further information on Nature Research policies, including our data availability policy, see Authors & Referees and the Editorial Policy Checklist.

Experimental design

1. Sample size

Describe how sample size was determined.

Sample size was determined to be large enough to allow statistical significance claims.

2. Data exclusions

Describe any data exclusions.

No data exclusions.

3. Replication

Describe whether the experimental findings were reliably reproduced.

All experimental findings were reliably reproduced.

4. Randomization

Describe how samples/organisms/participants were allocated into experimental groups.

Samples were allocated to groups of a given genotype, detected by standard genetic/ genomic approaches. Otherwise samples were randomly selected within these groups.

5. Blinding

Describe whether the investigators were blinded to group allocation during data collection and/or analysis.

Phenotypic analyses was performed without taking into account the genotype of sample groups, when possible.

Note: all studies involving animals and/or human research participants must disclose whether blinding and randomization were used.

6. Statistical parameters

For all figures and tables that use statistical methods, confirm that the following items are present in relevant figure legends (or the Methods section if additional space is needed).

n/a	Confirmed	
☐	☒	The exact sample size (*n*) for each experimental group/condition, given as a discrete number and unit of measurement (animals, litters, cultures, etc.)
☐	☒	A description of how samples were collected, noting whether measurements were taken from distinct samples or whether the same sample was measured repeatedly.
☐	☒	A statement indicating how many times each experiment was replicated
☐	☒	The statistical test(s) used and whether they are one- or two-sided (note: only common tests should be described solely by name; more complex techniques should be described in the Methods section)
☐	☒	A description of any assumptions or corrections, such as an adjustment for multiple comparisons
☐	☒	The test results (e.g. *p* values) given as exact values whenever possible and with confidence intervals noted
☐	☒	A summary of the descriptive statistics, including central tendency (e.g. median, mean) and variation (e.g. standard deviation, interquartile range)
☐	☒	Clearly defined error bars

See the web collection on statistics for biologists for further resources and guidance.

Software

Policy information about availability of computer code

7. Software

Describe the software used to analyze the data in this study.

Microscopy images were prepared using ImageJ/Fiji and in some cases

were adjusted using Photoshop CS4 (Adobe Software). Electron microscopy images were acquired using FEI AutoSlice and View™ software. Movies were assembled using QuickTime Pro and Final cut Pro.

For all studies, we encourage code deposition in a community repository (e.g. GitHub). Authors must make computer code available to editors and reviewers upon request. The *Nature Methods* guidance for providing algorithms and software for publication may be useful for any submission.

Materials and reagents

Policy information about availability of materials

8. Materials availability

Indicate whether there are restrictions on availability of unique materials or if these materials are only available for distribution by a for-profit company.	All unique materials used are available from standard commercial sources or will be available from the authors upon request.

9. Antibodies

Describe the antibodies used and how they were validated for use in the system under study (i.e. assay and species).	No antibodies were used in this study.

10. Eukaryotic cell lines

a. State the source of each eukaryotic cell line used.	No eukaryotic cell lines were used in this study.
b. Describe the method of cell line authentication used.	No eukaryotic cell lines were used in this study.
c. Report whether the cell lines were tested for mycoplasma contamination.	No eukaryotic cell lines were used in this study.
d. If any of the cell lines used in the paper are listed in the database of commonly misidentified cell lines maintained by ICLAC, provide a scientific rationale for their use.	No eukaryotic cell lines were used in this study.

Animals and human research participants

Policy information about studies involving animals; when reporting animal research, follow the ARRIVE guidelines

11. Description of research animals

Provide details on animals and/or animal-derived materials used in the study.	Nematodes of the species Caenorhabditis elegans were used in this study.

Policy information about studies involving human research participants

12. Description of human research participants

Describe the covariate-relevant population characteristics of the human research participants.	No human researcher participants were used in this study.